Space Weather

RESEARCH ARTICLE
10.1029/2019SW002198

Special Section:
Space Weather Events of 4-10 September 2017

Solar Radio Burst Events on 6 September 2017 and Its Impact on GNSS Signal Frequencies

H. Sato[1], N. Jakowski[1], J. Berdermann[1], K. Jiricka[2], A. Heßelbarth[1], D. Banyś[1], and V. Wilken[1]

[1]German Aerospace Center, Neustrelitz, Germany, [2]Astronomical Institute, Czech Academy of Sciences, Ondrejov, Czech Republic

Abstract During the intense solar radio bursts on 6 September 2017, Global Navigation Satellite Systems (GNSS) signal interferences were observed at ground stations in the European longitude sector from 20°N to 70°N for all GNSS satellites in view including GPS, GLONASS, and Galileo. The solar radio noise reduced the signal-to-noise ratio with clear frequency dependence. The impact of the radio burst has been found at L2 and L5 frequencies, but not at L1 frequency. The ground observation of the solar radio spectrum between 1.0 and 2.0 GHz corresponds well to such frequency dependence. The maximum signal-to-noise ratio reduction of -10 dB was found when the solar radio flux was pulsating around 2,000 solar flux unit level. Precise point positioning results show that accuracy is reduced with stronger deviation for dual-frequency solutions than for single-frequency solutions based on L1 signal only. The positioning error refers rather to the solar extreme ultraviolet flare than to solar radio interferences. The results presented here are a clear indication of frequency-dependent GNSS performance degradation during strong space weather events.

Plain Language Summary The sun occasionally emits strong radio waves during the evolution of active solar regions. This phenomenon was observed on 6 September 2017 around noon. We studied how solar radio waves can affect GPS signals. We found that the solar radio waves affected a subset of GPS frequencies and considered its influences on GPS-based applications. This study helps to understand the impact of solar radio bursts on satellite signals.

Key Points:
- Strong L-band solar radio bursts associated with a severe solar flare interfered with GNSS signal frequencies at L2/L5
- The observed GNSS SNR reduction due to the radio bursts is not considered as the primary source of signal tracking loss
- Dual-frequency positioning was more affected than single-frequency positioning

Correspondence to:
H. Sato,
hiroatsu.sato@dlr.de

Citation:
Sato, H., Jakowski, N., Berdermann, J., Jiricka, K., Heßelbarth, A., Banyś, D., & Wilken, V. (2019). Solar radio burst events on 6 September 2017 and its impact on GNSS signal frequencies. *Space Weather*, *17*. https://doi.org/10.1029/2019SW002198

Received 11 MAR 2019
Accepted 5 MAY 2019
Accepted article online 18 MAY 2019

1. Introduction

Space weather effects on Global Navigation Satellite Systems (GNSS) are predominately associated with degradations of L-band (1.0–2.0 GHz) signal phases and amplitudes. Extreme solar flares are space weather events with strong influence on GNSS signal propagation at the dayside, having an impact on the quality of satellite communication and navigation. Solar flares emit electromagnetic waves in a broad wavelength spectrum including X-rays, extreme ultraviolets (EUVs), and radio waves, causing an impact on GNSS signals through the following direct and indirect ways.

Solar EUV radiation is the major source of ionization in the Earth's upper atmosphere. Ionization due to EUV flares causes sudden changes in electron density along satellite-receiver links, which result in unexpected signal delays and degradation of GNSS application performance. The EUV impact on the differential carrier phase appears as a sudden increase in total electron content (TEC). TEC responses are closely related to solar EUV flux enhancements, especially good correlations have been reported for the 26- to 34-nm wavelength range (e.g., Le et al., 2013; Tsurutani et al., 2005). On the other hand, solar radio bursts may be composed by intense radio fluxes that exceed those observed under quiet solar conditions by several orders of magnitude. Such extreme radio burst events in the L-band frequency range can directly interfere with GNSS signals.

After early work by Klobuchar et al. (1999), the threat of solar radio bursts to GNSS signals became more widely recognized, showing that the signals interfere with solar radio flux, reducing the signal-to-noise ratio (SNR) of GPS signals (Cerruti et al., 2006). A number of L-band solar radio bursts in December 2006 have been extensively studied in respect to GPS interference occurrence (Carrano et al., 2009; Cerruti et al., 2008; Kintner et al., 2009). For the X class flare event on 6 December 2006, a notable difference between the L1 and L2 frequencies was recorded. When the solar radio burst near the L2 frequency was approximately 2 orders of magnitude lower compared to L1 (Carrano et al., 2009), the SNR effects were not visible at L2 frequency (Cerruti et al., 2008).

There are sometimes discrepancies found between the solar peak flux times and those implied by the GPS signals (Kintner et al., 2009). This could be due to the fact that many of the previous studies compared GPS data to the solar radio frequency equaling about half of that between L1 and L2 (~1.4 GHz), which may differ from the solar radio frequency at GNSS frequencies when a huge spectral dynamic occurs. Direct comparison of solar radio and GNSS signal frequencies requires therefore high-frequency resolution of solar radio flux data, and such comparison has not yet been done.

A recent study shows that large solar radio bursts are not limited to the period around the sunspot maximum, and the authors also estimated that the occurrence of L-band solar radio bursts exceeding 100,000 solar flux unit (SFU) is about two events per decade (Giersch et al., 2017).

L-band frequency dependence to solar radio bursts must be considered as a potential threat to unexpected performance degradations for users of multifrequency GNSS. While the American GPS system has played a pivotal role as a core system in satellite navigation for a long time, other global and regional GNSS systems have undergone significant development in recent years, for example, the Russian GLONASS, the European Galileo, the Chinese Beidou, and the Japanese QRZZ. The availability of several systems providing signals on multiple frequencies is important for the future development of new and more stable applications, thereby increasing system performance for GNSS users.

It has been reported that a solar radio burst (SRB) event introduced large errors in both the horizontal and vertical dimensions in satellite positioning. The SRB effects on GNSS signals have been studied particularly for the event on 24 September 2011. Reductions in SNR for GPS L1C/A, L2P, and L2C signals were found in the sunlit hemisphere (Sreeja et al., 2013). Intriguingly, the authors also reported that GPS L2C was less affected than L1C/A and L2P signals. This SRB event resulted in degrade of accuracy in a precise point positioning (PPP) service (Sreeja et al., 2014). Later, Muhammad et al. (2015) studied the event with higher sampling GPS data (1 s) and assessed the impact of SRB on GPS signals including SNR, loss of lock, and phase tracking. It should be noted that these studies predominantly focused on SRB effects on GNSS performances and did not consider potential EUV flare effects.

During the 6 September 2017 space weather events, X class solar flare and radio burst occurred around 12 UT. Ionosphere responses for the EUV flare have been typically seen in the increase of TEC and impacts on GNSS signals (Berdermann et al., 2018; Yasyukevich et al., 2018). Yasyukevich et al. (2018) indicated that GNSS signals tracking loss were not affected by SRB by using 1.415-GHz San Vito solar radio data. To assess detailed GNSS signal response to L-band SRB events, higher time and frequency resolution are required in both GNSS and SRB data sets.

In this paper, we use high-resolution ground-based GNSS signal and solar radio measurements to investigate the impact of strong radio bursts and EUV flux during the 6 September 2017 X9.3 event. The solar radio observation is used to characterize the frequency gradient in the L-band solar radio burst by using 100-Hz solar radio flux data with frequency resolution of 4.7 MHz within the whole L-band (1–2 GHz). These data allow us to do a direct comparison of solar radio and GNSS L-band frequencies. We analyze GNSS amplitude interference and its effect on SNR on L1, L2, and L5 frequencies from 50-Hz GNSS receiver in the European sector from 20°N to 70°N latitudes. Although the GNSS data set is limited to the sunlit European longitude sector, we analyze SRB-induced GNSS amplitude interference in much higher time resolution than previous studies. In order to estimate the impact on GNSS application, the change in differential carrier phase due to EUV ionization and loss of signal data is taken into account. Finally, we implement position solutions based on single- and dual-frequency approaches to estimate the potential impact of frequency gradients in solar radio bursts on GNSS multifrequency applications.

2. Instruments and Measurements

2.1. GNSS

The GNSS measurement stations used in this paper consist of a high-rate JAVAD receiver with 50-Hz time resolution. The receivers are able to track GPS (L1, L2, and L5), GLONASS (L1 and L2), Galileo (E1 and E5a), and augmentation systems like EGNOS. DLR's Experimentation and Verification Network (Noack et al., 2005) is used for on-site data processing, real-time scintillation analysis, in order to ensure near-real-time supply with a 1-min resolution via the Ionosphere Monitoring and Prediction Center service (Berdermann

Table 1
Overview of the High-Rate GNSS Stations and the Solar Radio Observatories Used in the Analysis

	Location	Latitude	Longitude	Update (Hz)	GNSS Receiver	GNSS Antenna
GNSS	Neustrelitz, Germany (nz02)	53°19′N	13°04′E	50	Javad Delta G3T	Leica AR25
	Ramfjordmoen, Norway (rf01)	69°35′N	19°14′E	50	Javad Sigma G3T	Leica AR25
	Bahir Dar, Ethiopia (bd01)	11°34′N	37°23′E	50	Javad Delta G3T	JavadRingAnt-G
Solar radio	Ondrejov, Czech Republic	49°54′N	14°46′E	100	—	—
	San Vito, Italy	40°38′N	17°50′E	1	—	—

Note. GNSS = Global Navigation Satellite Systems.

et al., 2014). In this paper, we use 50-Hz dual-frequency GNSS raw data to calculate SNR and differential TEC on time scales, which allows us direct comparison with high resolution L-band solar radio burst data. An overview of the receiver and antenna types used is given in Table 1.

2.2. Solar Radio Flux

To analyze the L-band solar burst, we use data from the 0.8- to 2.0-GHz solar radio spectrograph from the Ondrejov Solar Observatory, Czech Republic, which is tuned to sweep 100 times per second over the entire observed frequency band. This corresponds to the time resolution of 10 ms. The observed frequency band is divided into 256 channels having a frequency resolution of 4.7 MHz. The data acquisition system is equipped with a 12-bit A/D converter, which makes it possible to distinguish between 4,096 flux levels. The spectrograph is fully automated, observing the sun on a daily basis from sunrise to sunset. The technical details of the spectrograph can be found in Jiřička and Karlický (2008). The Ondrejov solar spectrograph has saturation values of a few thousands of SFU. In order to characterize the size of the solar bursts, we compare Ondrejov data with 1-s Radio Solar Telescope Network San Vito solar radio flux at 1.415 GHz.

The solar radio flux is measured in SFU (solar flux units, 1 SFU = 10^{-22} Wm^{-2}/Hz). Quiet solar flux (no solar activity and no sunspots) is generated by background thermal emission and is at 1,500 MHz about 50 SFU. Solar radio bursts are associated with solar eruptions and cause rapid changes in solar radio flux of nonthermal origin, which can exceed the level of quiet solar conditions by several orders of magnitude.

2.3. EUV

The EUV flux data used in this paper have been obtained by the Extreme Ultraviolet Variability Experiment (EVE) instrument on board the NASA Solar Dynamics Observatory (SDO; Woods et al., 2012). The EVE provides the 5- to 105-nm solar EUV spectral irradiance measurements with 0.1-nm spectral resolution and with 10-s update rate.

3. Solar Observations

3.1. EUV Observation

Figure 1 shows the EUV flux ratio observed by SDO on 6 September 2017. The relative flux ratios of 17.1-, 25.7-, and 30.4-nm EUV wavelengths from Extreme Ultraviolet Spectrophotometer (ESP) instruments are shown as a function of time. We take the EUV value at 11:50 UT as a quiet time reference. These EUV fluxes started to increase at 11:55 UT. The 25.7-nm wavelength increased to more than 170% compared to the quiet level. The two lower wavelength components started to increase later than the 30.4-nm component, rising to a peak value around 12:05 UT. The 30.4-nm wavelength flux increased to 158% at 11:58 UT (first peak) and 170% at 12:01 UT (second peak). We compare the ionization level with the EUV and GNSS carrier phase measurement in section 4.1.

3.2. Solar Radio Burst Observation

Figure 2a shows the solar radio spectrum over the range of 1.0–2.0 GHz as a function of time between 11:55 and 12:16 UT observed at the Ondrejov Solar Radio Observatory. During this event, the Ondrejov radio spectrum recorded significant amplitude saturation and small-scale frequency structures within the L-band frequency range. From the spectrogram, we extract the solar radio frequency close to the GPS L1 (1.57542 GHz), L2 (1.2276 GHz), and L5 (1.17645 GHz) signals. Figure 2b shows the solar flux for 1.573, 1.227, and 1.175 GHz. For these frequencies, the saturation levels are 1,906, 2,139, and 1,795 SFU, respectively. The solar flux data show clear frequency dependence in the L-band range. Although the full picture above the

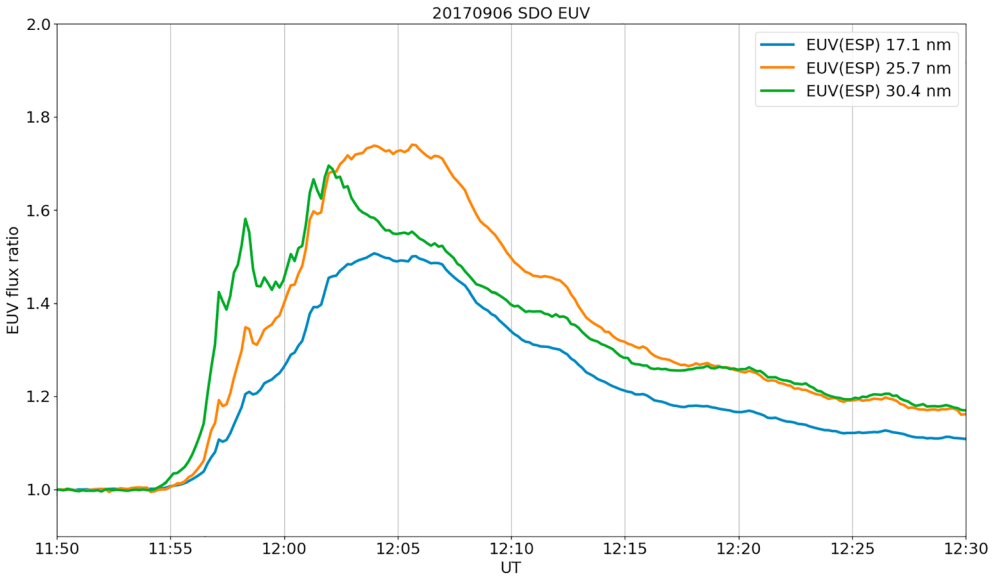

Figure 1. Extreme ultraviolet (EUV) flux ratio from Solar Dynamics Observatory (SDO) on 6 September 2017. The relative flux ratios of three EUV wavelengths from the EVE/ESP instruments are shown. The values at 11:50 UT are set as the reference.

saturation level cannot be seen, the amplitude of the solar radio flux is generally stronger for lower frequencies in this time interval. In order to give readers a perspective on the size of this solar radio bursts, we show Radio Solar Telescope Network San Vito 1.415-GHz solar flux in Figure 2c. In this solar radio frequency, the peak flux of 19600 SFU is recorded at 12:02:31.

There are two separate solar radio burst events that exceed the saturation limit of Ondrejov data within the given time interval. During the first event around 12:01–12:04 UT, the solar flux is constantly above the saturation level for all L-band frequencies. The L1 frequency component decreases to the normal level at

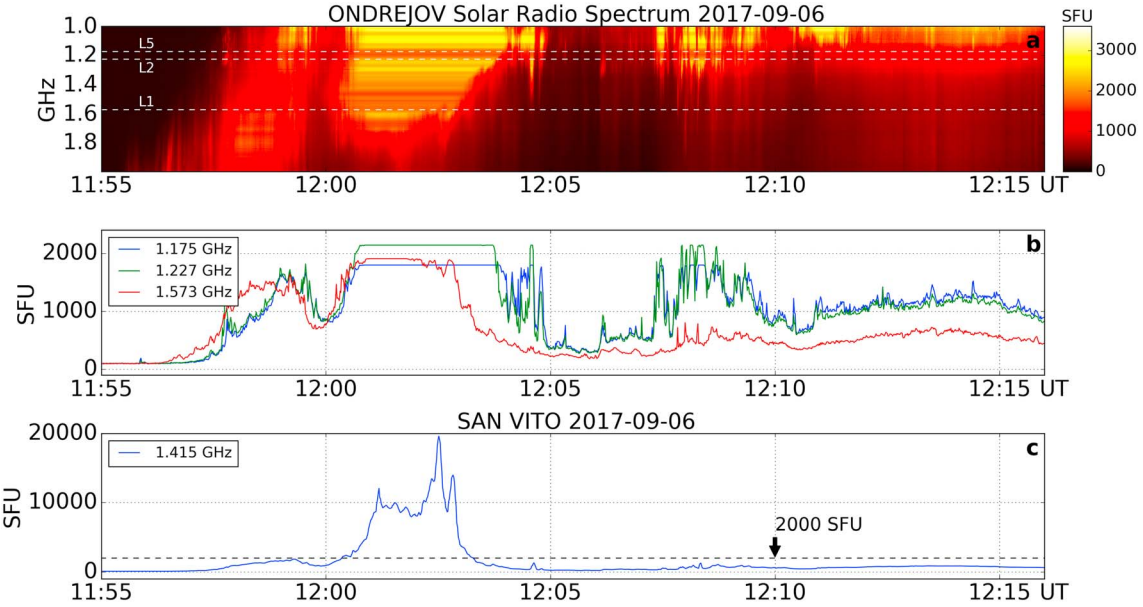

Figure 2. Solar radio observation on the 6 September 2017. (a) Ondrejov solar radio spectrum in the 1.0- to 2.0-GHz range. The GPS L1, L2, and L5 carrier frequencies are indicated by the dotted white lines. (b) Ondrejov solar radio flux intensity near the GPS frequencies. The flat curves after 12:01 UT correspond to the saturation levels of the solar radio frequencies. (c) Radio Solar Telescope Network San Vito 1.415-GHz solar flux. The dotted line indicates 2,000 solar flux unit (SFU) level for comparison with Ondrejov data.

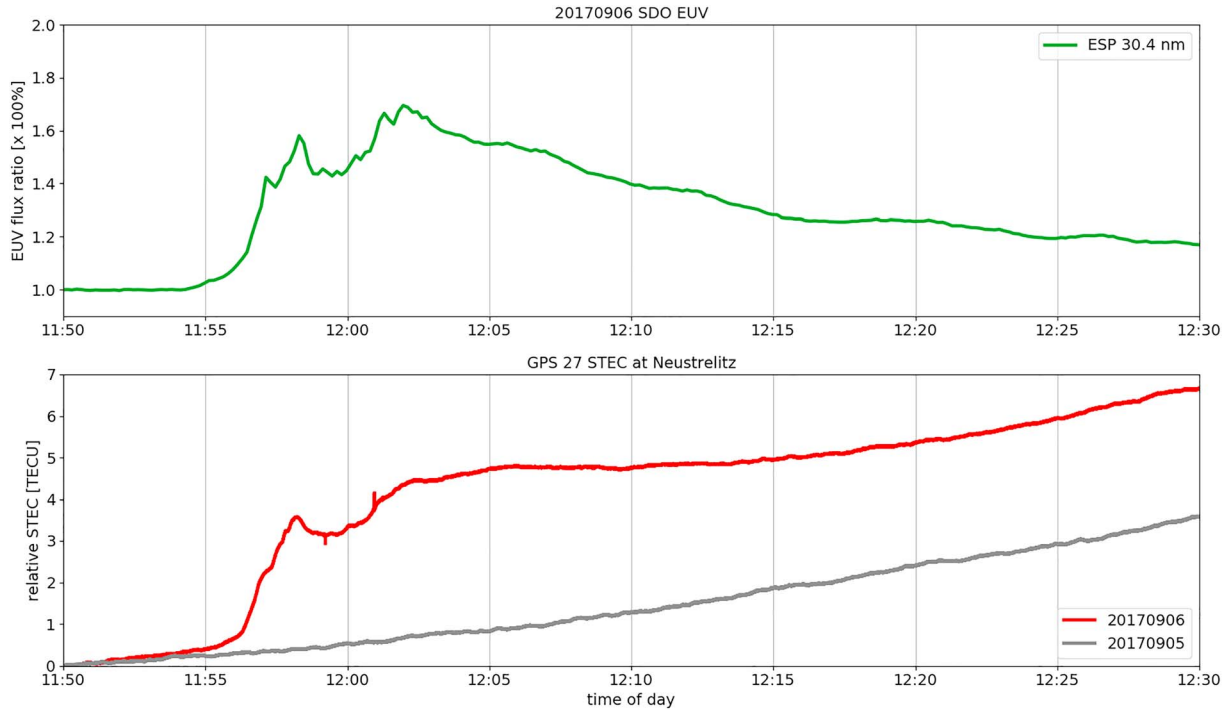

Figure 3. The extreme ultraviolet (EUV) 30.4-nm flux ratio from Solar Dynamics Observatory (SDO) from Figure 1 is shown (top) in comparison to the slant total electron content (STEC) measurement of the GPS 27 at the site Neustrelitz on 6 September 2017 (bottom, red line). The STEC on 5 September 2017 (bottom, gray line) is shown for comparison. The total electron content response to EUV fluxes is clearly visible.

12:03 UT while L2 and L5 components start to decrease at 12:04 UT with some fluctuations until 12:05 UT. The next strong burst event starts at 12:07 UT and lasts until 12:09 UT. During this event, only L2 and L5 components exceed the saturation levels. This event is characterized by strong amplitude fluctuations between the saturation limit and below the 1,000 SFU level within several seconds. From a radio astronomy point of view, this part of the burst is classified as "pulsations" (Jiřička et al., 2001). The solar radio flux recordings with the largest temporal increases are +796 SFU (1. 175 GHz) and +1,043 SFU (1. 227 GHz) per second, both recorded at 12:07:22 UT. The largest drops per second are −651 SFU (1. 175 GHz) at 12:04:39 UT and −849.55 SFU (1. 227 GHz) at 12:08:03 UT.

4. Impact on GNSS Signals

4.1. TEC Observation

Due to the enhanced EUV emission during the solar flare, a rapid increase of the TEC is expected. Slant TEC (STEC) measurements are calculated along the line of sight between the GNSS satellite and receivers based on the L1/L2 dual-frequency carrier phases. STEC represents the total number of electrons along the path in TECU [10^{16} electrons/m^2]. Here we use relative STEC from 50-Hz data (for the derivation of STEC; see, e.g., Kriegel et al., 2017).

Figure 3 shows the comparison of EUV flux and STEC measurement from GPS 27 at Neustrelitz on 6 September 2017. The 50-Hz GPS data are resampled to 1 Hz for the convenience of plotting. In order to highlight the STEC response to EUV ionization, the STEC measurement on 5 September 2017 is also shown as gray curve. The GPS geometry between the two paths is less than 2° in elevation. A clear response of STEC to the EUV ionization can be found for the 30.4-nm EUV wavelength. At 11:57 UT, the STEC increase is approximately 3 TECU above the reference value. The overall result corresponds well to the literature, where a good correlation between the 26.0- to 34.0-nm EUV band and the GPS TEC data (Le et al., 2013; Tsurutani et al., 2005) has been found. The STEC increases approximately 1 TECU per minute between 11:57 and 11:59 UT, and this satellite-receiver link-based observation agree well with Rate of TEC Index mapping (Berdermann et al., 2018).

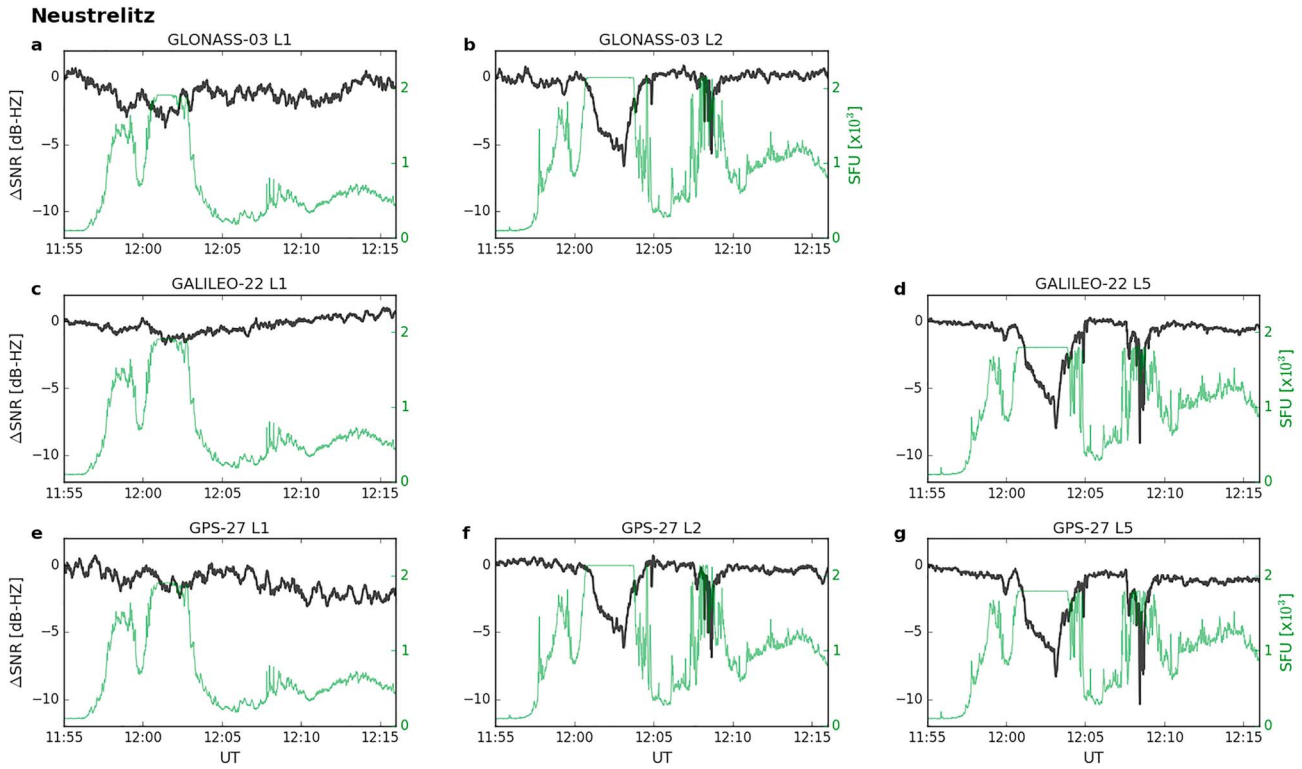

Figure 4. Global Navigation Satellite Systems amplitude interference under L-band solar radio bursts on 6 September 2017. The black curve shows signal-to-noise ratio (SNR) of GLONASS 03 L1 and L2 (a and b), GALILEO 22 L1 and L5 (c and d), and GPS 27 L1, L2, and L5 (e–g) recorded at Neustrelitz. Ondrejov solar radio intensity of corresponding L-band frequencies is shown by green curve. SFU = solar flux unit.

4.2. Radio Interference

The effect of solar radio bursts is usually seen in amplitude interference with GNSS signals. We use SNR data from 50-Hz GNSS receivers in the European sector to estimate solar radio noise effects. The SNR value is averaged per second using only satellite receiver links with an elevation threshold above 30° to avoid the influence of multipath effects on the amplitudes.

4.2.1. Frequency Dependence

Figure 4 shows the SNR of L1C/A, L2C, and L5 frequencies transmitted by the GPS 27, GLONASS 03, and Galileo 22 satellites recorded at the GNSS station at Neustrelitz Germany (53°19′N, 13°04′E). The SNR values at 11:55 UT are used as the reference values. L2 data from Galileo and L5 data from GLONASS are not available. The corresponding Ondrejov solar radio fluxes (see Figure 3b) are shown for comparison with GNSS SNR. Frequency dependence of solar radio interference is visible in the SNR data, which is correlated with the frequency gradient seen in the solar radio flux. There is no significant noise or fluctuations on the L1 frequency, but the SNR in L2 and L5 is reduced during the two intense solar radio flux events. A high correlation of the SNR and solar radio intensity levels has been found for all satellites in view. Figure 4 shows a direct experimental evidence of GNSS signal interference with corresponding L-band solar radio frequencies.

The largest reductions in SNR are found for the intense solar radio burst events between 12:01 and 12:04 UT and between 12:07 and 12:09 UT with greater effects for L5 than L2. Based on the reference value at 11:55 UT, GPS 27 SNR (L2) is reduced to −6.17 dB at 12:03:06 UT when the L2 solar flux is above the saturation limit and to −6.89 dB at 12:08:40 UT when the L2 solar flux is below the saturation limit. GPS 27 SNR (L5) is reduced to −8.32 dB at 12:03:09 UT where the L5 solar flux is above the saturation limit and to −10.36 dB at 12:08:27 UT when the L2 solar flux is below the saturation limit. There are small difference in SNR between L2C and L2P, where the L2C signal is degraded 0–2 dB more than L2P in average. This difference is not as significant as previous studies have shown (Sreeja et al., 2013).

We find the presence of pulsation in solar radio bursts can be distinguished by SNR behavior. SNR reduced continuously to below −5 dB between the intense solar burst 12:01 and 12:04 UT where solar radio flux was

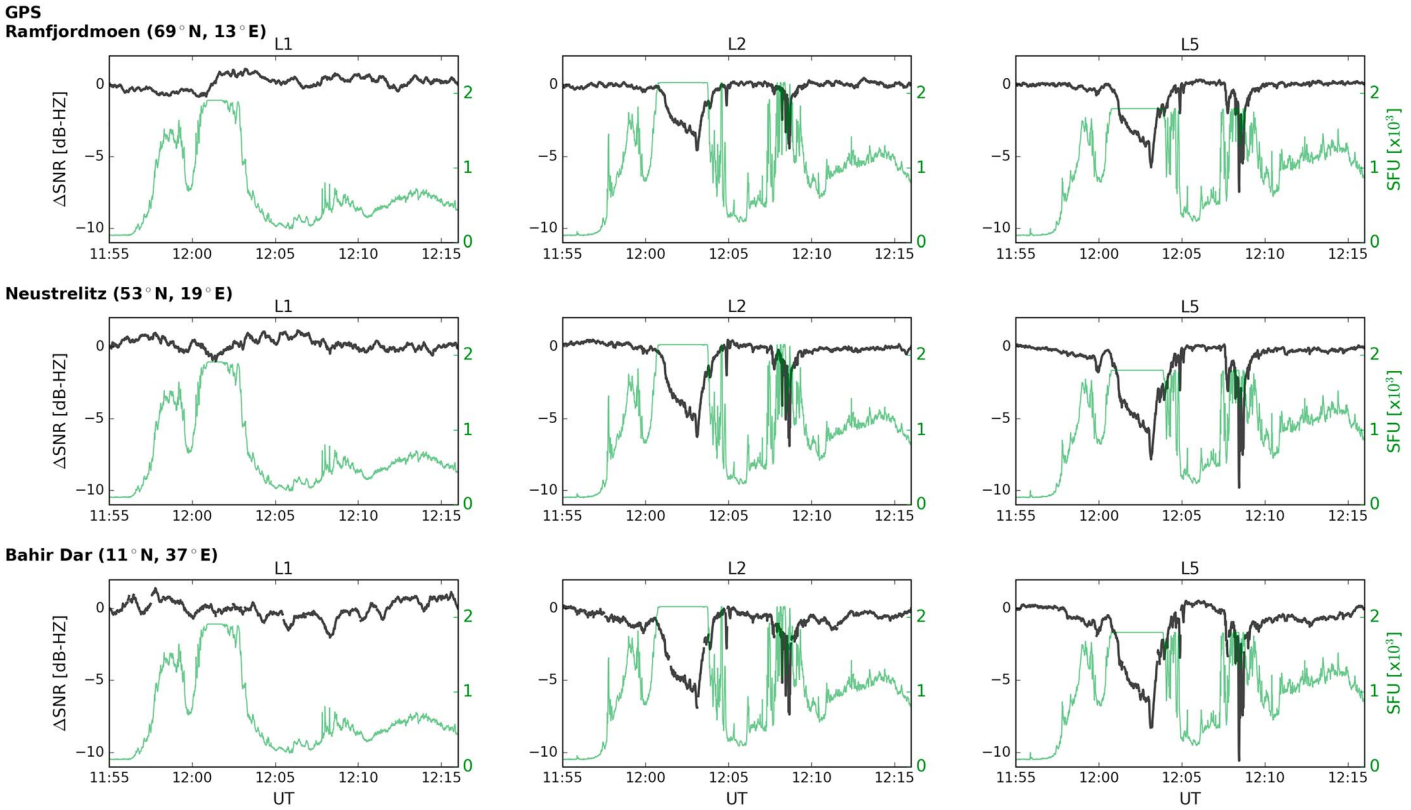

Figure 5. GPS amplitude interference under L-band solar radio bursts on 6 September 2017. The black curve shows average signal-to-noise ratio (SNR) of Global Navigation Satellite Systems L1, L2, and L5 frequencies from GPS satellites in view recorded at Ramfjordmoen, Neustrelitz, and Bahir Dar stations. The Ondrejov solar radio intensity of corresponding frequencies is shown by green curve. SFU = solar flux unit.

intense but without pulsation around the saturation levels. The rapid change of reduced SNR level for the L2/L5 frequency reflects well the corresponding solar radio spectrum pulsation. The largest SNR drops occurred during the solar pulsation between 12:07 and 12:09 UT both for L2 and L5. Although the saturation of Ondrejov data prevent us from estimating the maximum solar radio intensity in L2/L5 frequency during the solar pulsation events, these results indicate that significant SNR reduction is not only caused by large intensity but also depends on the pulsating behavior of solar radio bursts at the corresponding radio frequencies. The solar radio pulsation caused larger SNR reduction for GPS L2/L5 and GALILEO L5 frequencies. Among the interfered GNSS signals, SNR drop is most significant for GPS L5 and least significant for GLONASS L2 frequency.

SNR reductions to −10-dB level of GPS L2 frequency were observed for solar radio power larger than 10,000 SFU during previous SRB events (Cerruti et al., 2006, 2008). Figure 4 shows that this level of SNR reduction can be caused by much lower level of SRB if the radio flux intensity is fluctuating. The SRB intensity at L5 frequency was lower than 2,000 SFU between 12:07 and 12:09 UT on 6 September 2017.

4.2.2. Latitude Variation

To consider the latitudinal effect, we analyzed data from receivers installed at high, middle, and low latitudes in the European longitude sector. Figure 5 shows the GPS SNR of L1, L2, and L5 frequencies recorded at the GNSS stations in Ramfjordmoen (69°35′N, 19°14′E), Neustrelitz and Bahir Dar (11°34′N, 37°23′E). The SNR values are averaged over each L-band frequency. Similar to Figure 3, the Ondrejov solar radio fluxes are shown by green curves. The latitudinal dependence shown in Figure 5 is certainly due to the lower solar incidence angle at lower latitudes that enables stronger interference with GNSS signals. The solar radio effect on SNR reduction at Ramfjordmoen is lowest among the three stations, while the latitudinal difference between Neustrelitz and Bahir Dar stations is less significant. The irradiance angle effects on L1 and L2 frequencies have been discussed for previous SRB events (Carrano et al., 2009; Sreeja et al., 2013).

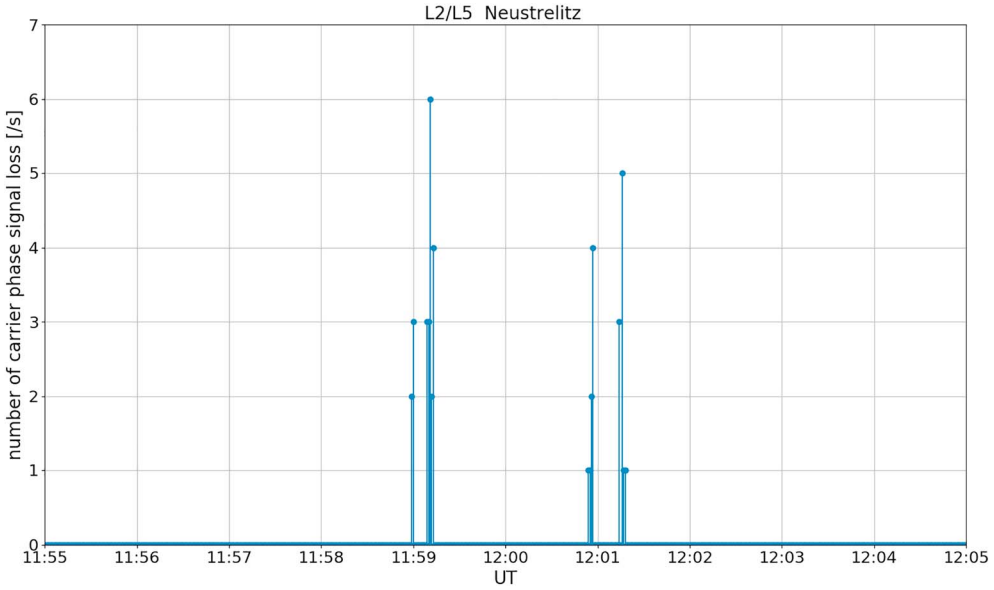

Figure 6. Occurrence of Global Navigation Satellite Systems L2/L5 carrier phase tracking loss at Neustrelitz between 11:55 and 12:16 UT on 6 September 2017. The number of signal loss instances is counted per second from 50-Hz data. No signal loss was observed on Global Navigation Satellite Systems L1 carrier phase.

While it has been reported that GPS L2 signals did not show clear solar irradiance angle effects during the 2011 SRB events (Sreeja et al., 2013), Figure 5 shows a clear solar irradiance effects for both GPS L2 and L5 between high and middle/low latitudes. The different behavior of this particular signal for 2011 and 2017 SRB events could be due to the available GPS data sets. The GNSS receiver used in this study has much higher time resolution and could track more GPS satellites with L2C signals. It should also be noted that the GPS L2 analyzed in Sreeja et al. (2013) are also from middle- to low-latitude stations and Figure 5 shows also smaller solar irradiance angle effects between middle- and low-latitude stations.

Although we cannot directly correlate the observed SNR with the solar radio burst intensity due to the saturation of the radio receiver, it is expected that there is a close correlation as indicated in the substructure at around 12:08 UT. To study the solar radiation impact on GNSS signals in more detail, the L-band radio flux receiver must be able to record a wide amplitude range to avoid saturation.

5. Impact on GNSS Performance

5.1. Carrier Phase Tracking

Here we analyze the occurrence of signal loss events during the solar radio burst at 11:55–12:16 UT. Figure 6 shows the number of signal loss events per second of GNSS L2 and L5 carrier phase from the 50-Hz receiver data recorded at Neustrelitz. The loss of L2 and L5 were recorded simultaneously for all the GNSS satellites. These events are found only in the time interval between 11:58:59 and 12:01:18 UT. The largest number of signal loss instances is found at 11:59:11 UT (six counts) and the second largest is at 12:01:16 UT (five counts). No signal loss was found for L1 carrier phase data. This distribution of loss of lock instances was identical for all GNSS satellites.

The time of signal loss generally coincides with the SRB and EUV events. At 11:59:11 UT, rapid fluctuations are found in the solar radio flux near the L2/L5 frequencies. The difference in solar radio intensity in L1 and L2/L5 is not significant. The solar radio noise seen in SNR reduction is not high. Therefore the solar radio flux may not be intense enough to explain why only the L2/L5 signals are affected. At 12:01:16 UT, the solar radio flux is more intense, and the solar noise level is higher for L2. But the SNR reduction is not yet significant compared to its peak value at 12:03 and 12:08 UT. A possible explanation is that L2 tracking is more likely affected by the same level of solar radio interference. The correlation between solar radio and L2 signal tracking loss has been reported before (Chen et al., 2005). In addition to solar radio flux, the EUV flare-induced ionization could also have been associated with the observed signal loss because the EUV flux

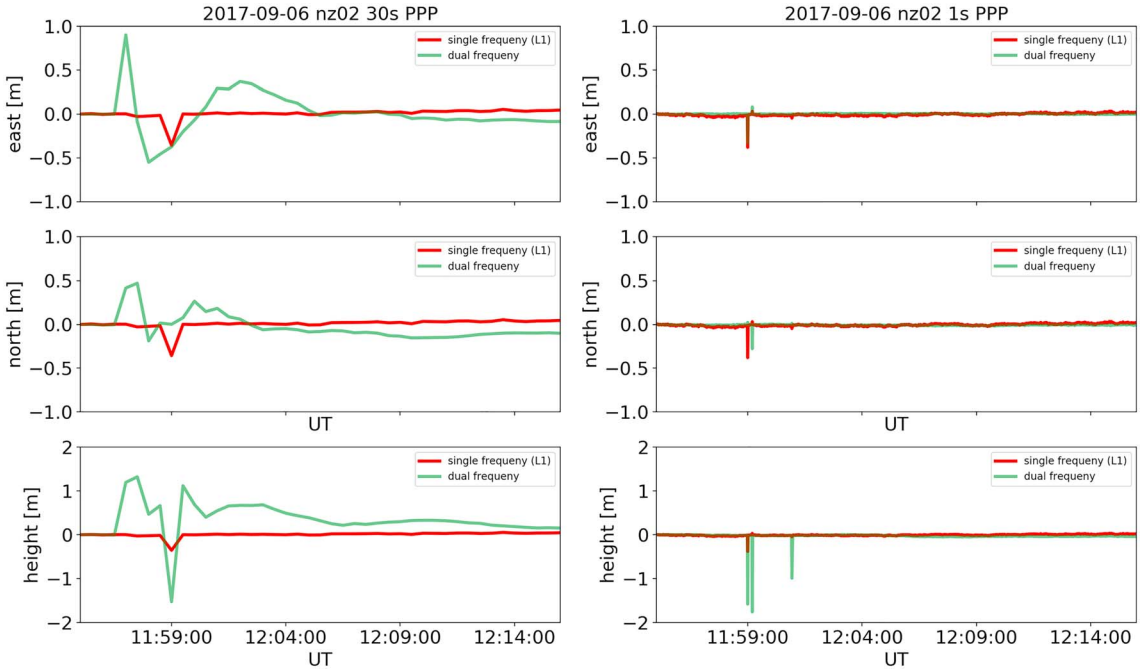

Figure 7. Dual-frequency and single-frequency precise point positioning (PPP) solutions for 30-s (left) and 1-s processing intervals (right) at Neustrelitz on 6 September 2017. The deviation from the reference coordinates is computed for east, north, and height in meters. The PPP processing was started at 00 UT in order to achieve sufficient convergence before solar extreme ultraviolet and radio burst events. The deviation is greater for dual-frequency solutions.

peaks were observed near the loss times. It is likely that both solar radio and EUV ionization contributed to the observed L2 loss of locks at receiver level. It should be noted that loss of signal sensitivity depends on the technical receiver performance. In fact, different behavior of GNSS receiver position filter reset was observed for 2011 SRB events (Sreeja et al., 2014).

5.2. Dual- and Single-Frequency Positioning

In this section, we present PPP results during the solar radio burst and EUV events on 6 September 2017. PPP is a phase-based GNSS technique that provides precise positions without additional observations from a reference station or reference station network. This method uses several corrections to compensate the satellite and station-dependent effects (Zumberge et al., 1997). To characterize the impact of the frequency dependency on GNSS applications, we compare two PPP solutions using dual frequency (L1 and L2) and single frequency (L1). The dual-frequency solutions use linear combination (ionosphere free combination) of the carrier phase and code observations of L1 and L2 to eliminate the ionospheric influence (first order). The algorithm prioritizes L2P than L2C when multiple signals are available. If only single-frequency observations on L1 are available, the influence of ionospheric signal delays may be mitigated with corrections from an ionospheric model (de Bakker & Tiberius, 2017; Wanninger & Hesselbarth, 2012).

For the following analysis we used the open source software RTKLib (http://www.rtklib.com) with the following correction parameters and settings: precise orbit and clocks (ftp://cddis.gsfc.nasa.gov/gps/products/1966), correction of the satellite antenna phase center offset, troposphere estimation, and solid Earth tides. IONEX files from the Center for Orbit Determination Europe (CODE) are used for the single-frequency solution. First, we calculated a reference solution, based on a 24-hr static dual-frequency PPP solution with the mentioned parameters and settings. The kinematic PPP solutions refer to this solution in the form of east, north, and height deviations. The dual-frequency PPP solution uses the linear combination to eliminate the ionospheric effect of the first order. Since the single-frequency PPP solution uses only the L1 frequency, the ionospheric corrections from CODE therefore have to be introduced to reduce the ionospheric influence.

Figure 7 shows the result of these two PPP solutions with 30- and 1-s observational data intervals. In order to examine the impact of the solar radio burst and EUV flare on position solutions, the PPP solutions were performed for the whole day so that the typical convergence time will not influence the positioning

performance for this time. For both processing intervals, the PPP solutions achieved less than decimeter accuracy at 11:50 UT.

The large deviations in the position have been found for both single- and dual-frequency solutions. For both processing intervals, the dual-frequency solution, which uses a linear combination of L1 and L2 observations, is more affected than the L1 single-frequency solutions. This result demonstrates that the L2 signals were more impaired than L1. The largest deviations of more than 1 m have been found for the dual-frequency solution in the height component, which leads to the typical GNSS behavior; that is, the different GNSS error sources affect the vertical more than the horizontal component. The times of deviation occurrence are different for both processing time intervals.

For the 30-s processing interval, the dual-frequency solution starts to deviate from the reference position for about 1 m at 11:57 UT, while the deviation in the single-frequency solutions occurred at 11:59 UT. For the 1-s processing interval, both dual- and single-frequency solutions deviate from the reference position at 11:59 UT. The magnitudes of the deviations are higher for longer time interval processing, which required a few minutes before reconvergence, while the impacts on 1-s solutions are limited to a few seconds.

Here we consider the possible trigger of the position deviations. At 11:57 UT, the abrupt changes in EUV flux led to the increase in STEC. The solar radio burst level also started to increase, but the intensity difference in L1 and L2 frequencies was not yet as significant as at later time, such as at 12:03–12:04 UT. Therefore, a possible explanation for greater deviation in the dual-frequency solution is that the L2 signal, which experienced stronger propagation effects, was significant enough to influence the first-order ionospheric correction. This interpretation can explain that the CODE model compensates well for the ionospheric effects on L1 and the single-frequency solution did not deviate until 11:59 UT for the 1-s solution.

The 1-s solutions were affected by the tracking loss of L2 carrier phase at around 11:59 and 12:01 UT. This result indicates that the PPP algorithm performs better against the frequency-dependent propagation effect due to the increasing levels of solar EUV and radio burst when higher-rate GNSS data are available, at least in the 1-s time intervals for this event. The result also allows us to conclude that the primary threat factor for high-rate PPP is the signal of loss in L2 during the event on 6 September 2017. The signal loss of L2 could be a result of the combined effect of the EUV flare and solar radio noises.

6. Conclusions

We have considered the strong solar radio bursts on 6 September 2017 around 12 UT and its impact on GNSS signals. During this event the solar radio flux was stronger in the GNSS L2/L5 frequency range than at L1 frequency. The GNSS data show a reduced SNR due to solar radio flux interference with L2 and L5 signals. We demonstrated that the pulsating solar radio burst in the scale of few thousand of SFU causes −10-dB SNR in the L-band. All the GNSS satellite systems in view were affected in a similar way, including GPS, GLONASS, and Galileo. The solar radio burst was associated with a solar EUV flare, which caused a prompt ionization enhancement in the Earth's upper atmosphere. As a consequence, the TEC calculated from GNSS dual-frequency carrier phases increased in parallel. The observations do not allow conclusions concerning the effect of the solar radio burst on the carrier phases. Since the observed tracking loss of L2/L5 carrier phases did not occur during the phase of highest solar radio noise, it is assumed that the rapid EUV and associated ionization enhancement primarily causes the loss of lock. A combination of EUV and SRB impact on GNSS signals is possible. Finally, we studied the impact of the radio burst/EUV flare on GNSS positioning by using dual and single-frequency methods. The results show that the dual-frequency solution is more affected by the solar activity than the L1 single-frequency solution.

Acknowledgments
The authors gratefully acknowledge the provision of EUV data from SDO and solar radio data from Ondrejov Solar Observatory. The EUV data are available from the University of Colorado (http://lasp.colorado.edu/eve/data_access/evewebdata/products/). The authors appreciate the support from the EISCAT scientific association and Bahir Dar University for hosting and maintaining the GNSS stations in Ramfjordmoen and Bahir Dar. The real-time 1-min GNSS observation of IMPC service can be accessed online (http://impc.dlr.de). All data used within the publication are available from the long-term storage of the Institute of Communication and Navigation of the German Aerospace Center and are permanently provided via ftp access (SERVER: ftp.kn.nz.dlr.de; USER: "dlr79"; PASSWORD: "7uN3LaBZhebv"; folder name: AGU_SW_Sato_et_al_2019) or on request to the email address impc-uhd@dlr.de.

References

Berdermann, J., Jakowski, N., Hoque, M. M., Hlubek, N., Missling, K. D., Kriegel, M., et al. (2014). Ionosphere monitoring and prediction center (IMPC), in *27th International Technical Meeting of the Satellite Division of the Institute of Navigation, ION GNSS 2014*, vol. 1, pp. 14–21, Tampa, Florida.

Berdermann, J., Kriegel, M., Banyś, D., Heymann, F., Hoque, M. M., Wilken, V., et al. (2018). Ionospheric response to the X9.3 Flare on 6 September 2017 and its implication for navigation services over Europe. *Space Weather*, *16*, 1604–1615. https://doi.org/10.1029/2018SW001933

Carrano, C. S., Bridgwood, C. T., & Groves, K. M. (2009). Impacts of the December 2006 solar radio bursts on the performance of GPS. *Radio Science*, *44*, RS0A25. https://doi.org/10.1029/2008RS004071

Cerruti, A. P., Kintner, P. M., Gary, D. E., Lanzerotti, L. J., De Paula, E. R., & Vo, H. B. (2006). Observed solar radio burst effects on GPS/wide area augmentation system carrier-to-noise ratio. *Space Weather*, *4*, 810006. https://doi.org/10.1029/2006SW000254

Cerruti, A. P., Kintner, P. M., Gary, D. E., Mannucci, A. J., Meyer, R. F., Doherty, P., & Coster, A. J. (2008). Effect of intense December 2006 solar radio bursts on GPS receivers. *Space Weather*, *6*, S10D07. https://doi.org/10.1029/2007SW000375

Chen, Z., Gao, Y., & Liu, Z. (2005). Evaluation of solar radio bursts' effect on GPS receiver signal tracking within International GPS Service network. *Radio Science*, *40*, RS3012. https://doi.org/10.1029/2004RS003066

de Bakker, P. F., & Tiberius, C. C. J. M. (2017). Real-time multi-GNSS single-frequency precise point positioning. *GPS Solutions*, *21*(4), 1791–1803. https://doi.org/10.1007/s10291-017-0653-2

Giersch, O. D., Kennewell, J., & Lynch, M. (2017). Solar radio burst statistics and implications for space weather effects. *Space Weather*, *15*, 1511–1522. https://doi.org/10.1002/2017SW001658

Jiřička, K., & Karlický, M. (2008). Narrowband pulsating decimeter structure observed by the new Ondřejov Solar Radio Spectrograph. *Solar Physics*, *253*(1–2), 95–101. https://doi.org/10.1007/s11207-008-9118-7

Jiřička, K., Karlický, M., Mészárosová, H., & Snížek, V. (2001). Global statistics of 0.8-2.0 GHz radio bursts and fine structures observed during 1992-2000 by the Ondřejov radiospectrograph. *Astronomy and Astrophysics*, *375*(1), 243–250. https://doi.org/10.1051/0004-6361:20010782

Kintner, P. M., O'Hanlon, B., Gary, D. E., & Kintner, P. M. S. (2009). Global Positioning System and solar radio burst forensics. *Radio Science*, *44*, RS0A08. https://doi.org/10.1029/2008RS004039

Klobuchar, J. A., Kunches, J. M., & VanDierendonck, A. J. (1999). Eye on the ionosphere: Potential solar radio burst effects on GPS signal to noise. *GPS Solutions*, *3*(2), 69–71. https://doi.org/10.1007/PL00012794

Kriegel, M., Jakowski, N., Berdermann, J., Sato, H., & Mersha, M. W. (2017). Scintillation measurements at Bahir Dar during the high solar activity phase of solar cycle 24. *Annales de Geophysique*, *35*(1), 97–106. https://doi.org/10.5194/angeo-35-97-2017

Le, H., Liu, L., Chen, Y., & Wan, W. (2013). Statistical analysis of ionospheric responses to solar flares in the solar cycle 23. *Journal of Geophysical Research: Space Physics*, *118*, 576–582. https://doi.org/10.1029/2012JA017934

Muhammad, B., Alberti, V., Marassi, A., Cianca, E., & Messerotti, M. (2015). Performance assessment of GPS receivers during the September 24, 2011 solar radio burst event. *Journal Space Weather and Space Climate*, *5*, A32. https://doi.org/10.1051/swsc/2015034

Noack, T., Engler, E., & Klähn, D. (2005). High rate performance, assessment of GNSS raw data based on the DLR experimentation and verification network, in *Proceedings of the 18th International Technical Meeting of the Satellite Division of The Institute of Navigation (ION GNSS 2005)*, pp. 13–16, Long Beach, CA.

Sreeja, V., Aquino, M., & de Jong, K. (2013). Impact of the 24 September 2011 solar radio burst on the performance of GNSS receivers. *Space Weather*, *11*, 306–312. https://doi.org/10.1002/swe.20057

Sreeja, V., Aquino, M., De Jong, K., & Visser, H. (2014). Effect of the 24 September 2011 solar radio burst on precise point positioning service. *Space Weather*, *12*, 143–147. https://doi.org/10.1002/2013SW001011

Tsurutani, B. T., Judge, D. L., Guarnieri, F. L., Gangopadhyay, P., Jones, A. R., Nuttall, J., et al. (2005). The October 28, 2003 extreme EUV solar flare and resultant extreme ionospheric effects: Comparison to other Halloween events and the Bastille Day event. *Geophysical Research Letters*, *32*, L03S09. https://doi.org/10.1029/2004GL021475

Wanninger, L., & Hesselbarth, A. (2012). *SBAS based single and dual frequency precise point positioning*, (pp. 3735–3741).

Woods, T. N., Eparvier, F. G., Hock, R., Jones, A. R., Woodraska, D., Judge, D., et al. (2012). Extreme ultraviolet variability experiment (EVE) on the Solar Dynamics Observatory (SDO): Overview of science objectives, instrument design, data products, and model developments. *Solar Physics*, *275*(1–2), 115–143. https://doi.org/10.1007/s11207-009-9487-6

Yasyukevich, Y., Astafyeva, E., Padokhin, A., Ivanova, V., Syrovatskii, S., & Podlesnyi, A. (2018). The 6 September 2017 X-class solar flares and their impacts on the ionosphere, GNSS, and HF Radio Wave Propagation. *Space Weather*, *16*, 1013–1027. https://doi.org/10.1029/2018SW001932

Zumberge, J. F., Heftin, M. B., Jefferson, D., Watkins, M. M., & Webb, F. H. (1997). Precise point positioning for the efficient and robust analysis of GPS data from large networks. *Journal of Geophysical Research*, *102*(10), 5005–5017. https://doi.org/10.1029/96JB03860